# An objectively selected case heavy rain event in the Western Mediterranean Basin: A study through diagnosis and numerical simulations

Martín M. L.[1], Santos-Muñoz D.[2], Morata A.[2] and Luna M. Y.[2]

[1]*Dpto. Matemática Aplicada. Escuela de Informática. Campus de Segovia. Universidad de Valladolid, Pza. Sta. Eulalia, 9-11, 40005 Segovia. Spain.*

[2]*Instituto Nacional de Meteorología. Leonardo Prieto Castro, 8. 28040 Madrid. Spain.*

***Corresponding author:*** *M. Yolanda Luna*
*Address: Instituto Nacional de Meteorología. Servicio de Desarrollos Climatológicos.*
*Leonardo Prieto Castro, 8. 28040 Madrid. Spain.*
*Email:* yluna@inm.es
*Phone: 34 915819703*
*Fax: 34 91 5819767*

## ABSTRACT

The heavy rain event of 8 to 21 November 2001 in the western Mediterranean area is objectively selected by means of a Singular Value Decomposition Analysis (SVDA) between 300 hPa large-scale (geopotential and u- and v-wind components) fields and regional precipitation. The flash flood episode corresponds to the highest expansion coefficient value of the second SVD mode. The second singular mode presents a heterogeneous geopotential pattern characterised by a centre of positive anomalies in the eastern North Atlantic in between two negative anomaly centres to southern of the Azores Islands and over Algeria. Synoptically, the episode is characterised by the presence of a long-lived Ω blocking geopotential pattern showing strong similarity with the obtained statistically mode highlighting the strength of the link synoptic variables-regional precipitation and revealing that the methodology was been able to capture such catastrophic flash flood event. The jet streak interaction during most of the episode was crucial for triggering and driving of the deep convection. A set of mesoscale numerical simulations using MM5 is performed to investigate the mechanisms responsible for the convection development through several output diagnosis. A potential vorticity evolution show how dry air masses are extruded from the stratospheric levels promoting strong cyclonic circulation at all levels as is noted in 500 hPa relative humidity maps. A deep vertical column of high relative humidity over the Algerian coastline supports the few and geographically confined convective cells responsible for the heavy precipitation over different zones at the study area. The study of mesoscale environment parameters showed an enhanced conditional unstability through a deep troposphere layer with strong vertical wind shear that favoured conditions to allow organization of long-lived convective structures.



Keywords: heavy rain, western Mediterranean, singular value decomposition, mesoscale model.

## 1. Introduction

Due to the distinctive orography of Iberia the Western Mediterranean climate is confined to a narrow coastal strip of land spanning southwest France, the eastern Iberia coastline and western North Africa. The strip is characterised by an abrupt rise of land from the coast with an area made up of high mountains, which rise to varying heights at no great distance inland. The Western Mediterranean area presents extreme contrasts between warm and cold seasons. While the Azores High dominates the zone during the warm season with hot and very dry weather, travelling disturbances associated with the mid-latitude westerlies reinforce the moderate and appreciate weather during the cold season. Moreover, the closed characteristic of the Mediterranean Sea and the high insolation received during long part of year lead to high sea surface temperatures during summer and autumn which ensure very warm, moist air to be forced to rise over the orography. This situation favours instability and the release of vast amounts of latent heat. The result is the development of thunderstorms which may be a single supercell, a squall line or the presence of secondary cyclones over the Mediterranean. In particular, the southeast of Spain with annual average precipitation totals as low as 150 mm (Wheeler 1989) constitutes the driest area not only of Iberia but also of Europe and offers a landscape more similar to neighbouring Africa.

Dramatic swings in precipitation constitute one of the dominant forms of climate variability in the eastern Iberian Peninsula. The Western Mediterranean is particularly characterised by floodings during the late summer and autumn and dry periods lasting up to several years (Doswell et al. 1998; Romero et al. 2000). Several physical and dynamical processes, such as storm track changes, low-level advection of warm, moist air or topographic configuration can play an important role in autumn extreme episodes (Font, 2000). Numerical simulation of case studies has shown that coastal orography results one of the decisive factors in the localisation and spatial distribution of the rainfall (Romero et al., 1997; Romero et al., 1998). At the end of summer and at the beginning of autumn, strong and unstable phenomena show up over both land and sea, because of polar air advection associated with disturbances developing in the proximity of the Mediterranean (Linés, 1970). Most of these disturbances usually affect the Mediterranean Iberian

coast and the Balearic Islands and cause the heaviest and most important precipitation from September to November. Going deeply into the importance of this line of research is beyond the pure scientific domain since socioeconomic impacts of such extreme episodes are far from negligible (IPCC Technical Summary, 2001).

Although other factors such as sea surface temperature, land-sea effects, topographic configurations, etc, can be important in explaining precipitation anomalies, Valero et al. (2004), hereafter VAL04, and Martín et al. (2004) have demonstrated that the influence of upper-level large-scale circulation on the precipitation in the Western Mediterranean is very significant. The 300 hPa level is highly related to jet streams which are usually located near the tropopause level, hence the use of this level allow us to check if dynamics associated to the statistically derived flow patterns is consistent with the atmospheric structure revealed by the geopotential height and complemented with that of the wind components. The wind components inform about jet streams with a strong meridional component associated to cut-off lows, one of the main dynamic mechanisms for developing precipitating systems in the Western Mediterranean Basin (Valero et al., 1997). Taking into account these studies, this paper is devoted to deeply analyse the features conducing to heavy rainfall episodes from the linkage between the Western Mediterranean Basin precipitation fluctuations and the large-scale circulation anomalies during the autumn season using observational data. We have considered a case of heavy rainfall over the western Mediterranean area that has been objectively selected and analysed from the singular value decomposition analysis applied to large-scale upper-level atmospheric variables, such as geopotential height and horizontal wind components at 300 hPa, and western Mediterranean autumn precipitation. The purpose of this paper is to identify atmospheric circulation patterns occurring simultaneously with precipitation anomaly configurations and to also analyse synoptic and mesoscale mechanisms that explain the episode. The simulations will be useful to help forecasters to monitor the area suggesting a general scenario for those key features that play a significant role in developing such heavy rain events.

The study is organised as follows. A description of the datasets is given in Section 2. Section 3 is devoted to describe the methodology for selecting the case study. Section 4 briefly describes the non-hydrostatic mesoscale model used to diagnose the meteorological situation. Section 5 focuses on the analysis of the objectively selected heavy rainfall events in the western Mediterranean area. The summary and discussion of the main results are drawn in Section 6.

## 2. Data

Initially, the data employed in this study include geopotential height (Z300) and horizontal wind (U- and V-wind) components at 300 hPa. These data and the sea level pressure (SLP) are chosen from NCEP Reanalysis (Kalnay et al., 1996). The data are monthly means over a 2.5º x 2.5º grid of 54-autumn (September-October-November) seasons for the period 1948-2001. In a first step, for all datasets the selected domain for this study spans the North Atlantic Ocean, the Mediterranean Sea and Europe from 20º to 80ºN, and from 100ºW to 40ºE. Figure 1 shows the locations of the precipitation data (PCP) that were extracted from the database of the Spanish Meteorological Service (Instituto Nacional de Meterología, INM). The rainfall data consists of time series of 16 sites (1948-2001) covering the Mediterranean coast of the Iberian Peninsula and the Balearic Islands. Prior to the diagnostic analysis, all large-scale data sets are modified applying a cos(latitude) square root area-weighting to account for the uneven spatial density of the grid. The original data were also detrended and the seasonal cycle was removed by subtracting the long-term mean to each monthly value. Finally, standardised anomalies were obtained for all fields.

To deeply analyse the case study, daily geopotential height, sea level pressure, horizontal wind components, relative humidity, temperature are also used at several atmospheric levels. These data are also extracted from NCEP Reanalysis over the same 2.5º x 2.5º grid for the selected domain. Moreover, other products are derived from these data and analysed for the whole heavy rainfall period. The precipitation data corresponding to the episode are also extracted from the same database of the Spanish Meteorological Service.

## 3. Methodology for selecting a case study: SVD Analysis

To avoid bias, the selection of a case study should not be made subjectively. We have objectively chosen a case by a classification scheme based on the Singular Value Decomposition Analysis (SVDA) trying to find a relationship between the large-scale circulation and the precipitation conducing to heavy rainfall episodes in the Western Mediterranean Basin. Here, we only give a brief description of the method. Nevertheless, if more details about SVDA are required, they can be found in Bretherton et al., (1992) and Storch and Zwiers (1999). The SVDA can be thought of as a generalisation of the diagonalisation of a square symmetric matrix to the diagonalisation of a rectangular one, i.e., it is a generalisation of empirical orthogonal functions (EOF) analysis (Lorenz, 1956; Davis, 1976). SVDA has been usually applied to two data fields together in order to identify modes that explain the greatest covariance between such fields. A SVD of the cross-covariance matrix of the two data fields yields two sets of orthogonal patterns describing a squared covariance fraction (SCF) of two time series. These patterns are called left and right singular vectors. Moreover, those modes are ordered with respect to their singular values so that the first pair accounts for the largest SCF and the remaining pairs describe a maximum fraction unexplained by the previous pairs (in analogous manner to the eigenvalues in EOF). Each singular value measures the contribution of each corresponding pair of modes to the total squared covariance. Thus, the SCF accounted for by the i-*th* pair of singular vectors is proportional to the square of its singular value. If the i-*th* singular vector is projected onto each data field, the i-*th* expansion coefficient for each variable can be obtained. The correlation between the i-*th* expansion coefficients of the two variables measures the intensity in the relationship between the pairs. The heterogeneous correlation pattern for the i-*th* left (right) field is defined as the correlation between the left (right) field and the i-*th* expansion coefficient for the right (left) field. For display purposes, the time series of expansion coefficients have been normalised by their standard deviation and the corresponding heterogeneous correlation patterns have been multiplied by the data standard deviation so that each SVD spatial pattern represents anomalies.

The SVDA was then performed on the detrended data obtaining seasonally-independent detrended modes. The expansion coefficients are obtained by

projecting the original data (i.e., non-detrended) onto the previously derived SVD spatial modes. This allows for a representation of the long term trends in the time series of expansion coefficients while the initial detrending of data avoids inflation of the cross-covariance coefficients in the determination of the spatial SVD patterns (Heyen et al., 1996). To further examine heavy rainfall episodes, real situations are directly extracted from months with the highest expansion coefficient values because they indicate situations in which the corresponding mode is dominant.

The SVDA has been carried out diagonalising three covariance matrices derived between the monthly geopotential height-, the zonal wind component- and the meridional wind component- and the precipitation field, i.e., diagonalising (Z300-PCP), (U300-PCP) and (V300-PCP) for 54-autumn seasons. In VAL04, we presented the results for 42-autumn seasons (1948-1989) associated with these three diagonalizations showing special interest in the two first coupled modes. The analysis of these two leading modes suggested that the large-scale atmospheric circulation at 300 hPa is responsible of much of the signal related to the western Mediterranean precipitation. If more details about the SVD results are required, they can be found in VAL04. The implementation of the above described methodology in this paper has allowed an episode of heavy rainfall to be objectively selected to analyse the main atmospheric features conducing to heavy precipitation in the Western Mediterranean area. This episode has been associated with the second mode of covariability for the three matrices and it explains more than 21% of the squared covariance between large-scale and precipitation fields.

Figure 2 shows the expansion coefficient time series derived from the SVDA to (Z300-PCP), (U300-PCP) and (V300-PCP) matrices and associated with the second coupled mode. In general, there was a similar time evolution (correlation values higher than 0.64 significant at the 0.01 level) in the three cases. Moreover, similar variability patterns in regional precipitation were produced by the second SVD mode regardless of the considered large-scale variable (Z300, U-wind or V-wind) indicating that the same dynamic atmospheric structure is represented by that mode. The second mode spatial patterns of the SVDA to (Z300-PCP), (U300-PCP) and (V300-PCP) matrices are displayed in Figure 3. Figure 3a shows the Z300 patterns with a centre of positive anomalies in the eastern North Atlantic in between

two negative anomaly centres to southern of the Azores Islands and over Algeria. In this situation E-NE air flow is advected over Iberia favouring negative precipitation anomalies over the northeast Iberia and positive ones over the southeast of Iberia and the Balearic Islands as reflects the precipitation anomalies pattern (Fig. 3b). The described northeastern advection over Iberia can be noted in Figure 3c corresponding to the U-wind pattern. An area of negative anomalies centred about 40ºN latitude over the Iberian Peninsula and two positive nodes to northwestern of Great Britain and to southeastern of the Atlas Mountains can be observed. The associated precipitation pattern (Fig. 3d) closely resembles the configuration displayed in Figure 3b with a value of spatial correlation of 0.97 between both patterns. Finally, the results of the SVDA applied to the V-wind component and precipitation fields are shown in Figure 3e. A west-east dipolar configuration in the anomaly pattern for the meridional wind arises. The distribution pattern is related with reinforcement of the north wind component over Western Europe in agreement with the NE advection over Iberia described for the Z300 pattern and responsible for the dry conditions over the northeastern Iberia. In fact, in Figure 3f it can be noted that the precipitation pattern has strong similarity with the rainfall configurations displayed in Figures 3b and 3d with spatial correlations values of 0.90 and 0.86, respectively.

From the expansion coefficient time series (Fig. 2) derived from the SVDA to the three matrices and associated with the second coupled mode, the case of November 2001 was selected because of its highest expansion coefficient values. In Figure 4, we can see how both the large-scale (Figs. 2a, c and e) and the precipitation (Figs. 2b, d and f) expansion coefficient series, exceed the level of two standard deviations indicating high degree of coupling between the large-scale variables and regional precipitation. Further understanding of the heavy rainfall case demands an identification and evaluation of both synoptic and mesoscale processes involved in this episode. In this paper, our diagnosis will be assisted by means of the non-hydrostatic mesoscale model presented in the next section.

## 4. Diagnostic methodology: description of the mesoscale model

To deeply analyse the objectively selected case of heavy rainfall in the western Mediterranean area and to assist with our diagnosis, the non-hydrostatic mesoscale model (MM5, version 3) of the Pennsylvania State University-National Center of Atmospheric Research is used (Anthes and Warner, 1978; Grell et al., 1994). The model enhances vertical resolution in the lower troposphere to represent the boundary layer processes. It is formulated using the terrain following $\sigma$ coordinate system. The model has two-way interaction between successive nesting levels that allows realistic terrain characteristics (Zhang et al., 1986). In this paper, two interacting domains were used with 151 x 172 x 30 grid points. Figure 4, with fine grid domain and its orography, shows the centred domain in the eastern Iberia. This domain measures 1720 x 1510 km under a Lambert conformal map projection (10 km to horizontal spacing). On the other hand, Figure 5 shows the selected coarse domain. It measures 4530 x 3030 km and is centred at the same location. The time steps are chosen as 30 s and 90 s for the fine and coarse grids, respectively. The initial and boundary conditions for the coarse grid are taken from NCEP global reanalysis data (available at 00, 06, 12 and 18 UTC) with a resolution of 2.5 degrees. These fields are interpolated to the $\sigma$ model levels. The physical parameterisations of the model consist of the version of Reisner 1 explicit microphysics moisture scheme (Reisner et al., 1998) representing with predictive equations for cloud water and rainwater below the freezing level, and cloud ice, snow and supercooled water above the freezing level. Also allows slow melting of snow below freezing level and memory processes for cloud ice and snow. A look-up table for efficiency has been used. The Betts-Miller parameterisation scheme (Betts, 1986; Betts and Miller, 1986) is chosen to calculate moist convection effects on the coarse grid domain, whereas parameterised convection for the fine grid domain uses the Kain-Fritsch scheme (Kain and Fritsch, 1990). The scheme of Blackadar (1979) has been used for planetary boundary layer physics, a force-restore slab model to calculate the surface temperature over land keeping it constant over sea (Blackadar 1979; Zhang and Anthes, 1982; Zhang and Fritsch, 1986). Longwave and shortwave radiation effects are considered by the cloud cover (Benjamin, 1983). Two simulations for each day have been performed from 0000 and 1200 UTC till 0000 and 1200 UTC (next day), respectively. The integrations

start at 0000 UTC on 8 November 2001 and finish at 0000 UTC 22 November 2001.

## 5. Diagnosis of the case of November 2001

The western Mediterranean area is usually characterised by heavy rainfall in autumn (Maheras, 1988; Corte-Real et al., 1995; Sumner et al., 2001). Most of the situations conductive to heavy precipitation over that area are related to a broad scenario characterised by an upstream trough or closed low over the southwestern Iberia isolated from the general westerly regime or belonging to a blocking high-over-low pattern which occurs most frequently over the west coast of Europe (Font, 2000; Valero et al., 2004). Such large-scale distribution favours easterly air masses at low levels interacting with the coastal topography of eastern Iberia and contributes to heavy rainfall over the eastern Iberian coast. However, the case of November 2001 presents several differences. From the daily data and for this event, the heavy precipitation occurred over an extended period (8-21 November 2001) and mainly affected the northern of Africa and the Balearic Islands, with particularly heavy 24-h rainfall totals on 10 November over Algeria and on 11 November over the Balearic Islands. The eastern and southeastern Iberia were also affected but in minor intensity. The whole episode is analysed but it will be placed emphasize on the first part of the heavy rain event (from 8 to 12 November 2001) because the most devastating flash floods occurred on these dates. Figure 6 displays the total rainfall amounts and distribution of 8-12 November. It is highlighted precipitation values higher than 400 mm over the Algeria zone and values higher than 200 mm over the Balearic Islands. Taking into account that the fine grid domain used in this paper is 10 x 10 km, daily precipitation (not shown) became organised over small areas of Algeria and Balearic Islands. The rainfall maximum for the event was recorded in the Algeria coastline and exceeded 300 mm on 10 and 11 November with 140 mm on only six hours.

At surface (Fig. 7a), the situation at 1200 UTC 9 November is characterised at the surface by a meridionally extended high pressure zone located to the western British Island flanked by two low pressure centres at southern Genoa Gulf and at western Azores Islands, respectively. The stationary anticyclone with the Genoa

low, which presented an associated cold front, promote northern maritime cold air advection over the Iberian Peninsula. At 500 hPa (Fig. 7b), the synoptic distribution is similar to the surface distribution. However, it is remarkable how an initially centred trough (not shown) over the Scandinavia Peninsula at 1200 UTC 8 November becomes a retrogressive positively tilted and diffluent trough, and a cold core low is finally located over Algeria at 1200 UTC 10 November. This persistent and particular configuration reflects a blocking pattern named "Omega block" with a zonally oriented configuration of a high sandwiched in between two lows (Sumner 1954; Bluestein 1993). At upper level, this kind of configuration is usually characterised by a stationary ridge laying eastern Atlantic Ocean and by a main trough situated over the western Mediterranean zone which promotes meridional incursions of maritime cold air which comes from the central Europe and flows into the Western Mediterranean area after rotating around a cut-off low nearby the Iberian Peninsula. This strong low-index pattern is also related to a very strong meridional temperature gradient. Figure 8 displays on the fine grid domain a tongue of low temperature values on 10 November, 1200 UTC, spreading out along the whole Iberian Peninsula and north of Africa. In a sequence of diagnosed temperature maps (not shown), strong decrease of temperature in 24-h is noted, decreasing more than 12º C at most of the Iberian Peninsula and the northern Algeria. At middle and upper levels, the main low was elongated along the Algerian coast and exhibited a structure with two centres (not shown) in which the secondary centre was located over the Atlas Mountains. At 300 hPa (Fig. 7c), there was a jet streak from the north of Africa over the western Mediterranean area. The cold advection and the cyclonic vorticity on the right side of the jet stream entrance region merged to drive large-scale instability conditions that result in heavy precipitation over the southwestern Mediterranean region. Moreover, the interaction between airflow and a mountain ridge is stronger when the upper level winds are intense and nearly perpendicular to the ridge axis, as can be noted in Figure 7c (Smith, 1989).

A sequence of Potential Vorticity (PV) maps from 8 to 12 November at 300 hPa, 1200 UTC (Fig. 9) reflects a strong pool that progresses from the high latitudes to the western and central Mediterranean area spanning from the NW Iberia to the northern Africa. There are remarkable high values of PV units (higher

than 8 PVU) which indicate lowering of the dynamical tropopause and intrusions of stratospheric air. This PVU tongue represents PV anomalies (not shown) of great strength, depth and breadth which are associated with strong cyclonic circulation at all levels. In this situation, rapid pressure falls occurred at low levels in juxtaposition with the upper level jet streak (Holton, 1992; Barnes and Colman, 1994). The associated positive (negative) vorticity advection is situated ahead (rear) of the PV anomaly indicating that vertical upward (downward) motions will occur due to the increase of such advection with height. Consistent with the jet-induced upward forcing features, the model diagnoses upward vertical velocity throughout the troposphere. According to McGinley (1986), upward motions smaller than $0.5ms^{-1}$ are sufficient to trigger severe convective storms. Figures 10a and 10b shows two vertical cross sections of the relative humidity and the vertical motions on 10 and 11 November 2001. On 10 November at 1200 UTC (Fig. 10a), it can be noted a vigorous plume of upward motion extending from surface to 300 hPa over a narrow area of northern Africa. Another significant feature is the existence of a deep vertical column of high relative humidity spanning over the Algerian coastline which supports the few and geographically confined convective cells responsible for the heavy precipitation over different zones at the study area. On 11 November at 0600 UTC (Fig. 10b), it is highlighted another centre of intense upward motion over the Balearic area with a high relative humidity column throughout the troposphere over the same zone. As the quasigeostrophic theory, if the jet streak is near the tropopause, as in the November 2001 case, below jet-streak level vorticity advection becomes more cyclonic (anticyclonic) with height in the right (left) entrance region which is related to rising (downward) motion below such area. As a result downward motion, dry stratospheric air is transported into the higher levels of the troposphere. Figure 11 displays the relative humidity at 500 hPa on 11 November, 1200 UTC. It can be noted lower relative humidity values over western Iberia according with the dry air extruded from the stratospheric levels. On the contrary, over the right entrance jet region associated with vertical upward motions it is remarkable an extended area with higher values of relative humidity over the Atlas Mountains and the Spanish Mediterranean littoral.

Observed radiosoundings at Murcia and Palma de Mallorca stations have been used to describe the vertical troposphere structure. Thus, additional standard

tools of convective storm analysis, such as the totals-totals index (TTI), the lifted index (LI) and the K index (KI), have been computed from the radiosonde data (Galway, 1956; George, 1960; Miller, 1972). The evolution of the three indices indicate potential for convective storms reaching the TTI, LI and KI values of 45, 2 and 12, respectively at Murcia station and values of 50, 3 and 14, respectively at Palma station. From the soundings at the initial to the final storm period, increase in conditional instability is noted associated with differential temperature and moisture advection. Figures 12a-c show the Palma soundings on 9, 10 and 11 November as the most representative of the heavy rain episode. In Figure 12a a surface-based inversion is shown and the dewpoint line emphasizes the dryness of the 1000-300 hPa layer related to intrusions of stratospheric air. If we set the Figure 12a against the corresponding 10 November sounding (Fig. 12b), it is remarkable how some increase in conditional instability is noted associated with differential temperature and moisture advection. Figure 12b shows up a shallow surface-based, nearly adiabatic and well-mixed layer characterized by easterly flows carrying moist air off the Mediterranean Sea. This layer is separated from a dry, cold layer above. According to Bluestein (1993), the dry air aloft suggest that the potential for negatively buoyant and cooled downdrafts favoured that liquid precipitation mixes with the environmental air. Furthermore, the wind shear is non-unidirectional and the wind shear vector is veering with height as displayed in Figure 12b. According with Klemp and Wilhelmson (1978), the development of a severe right-moving storm is favoured creating updraft intensification in such a frame. Throughout the episode, large values of vertical wind shear higher than 50 $ms^{-1}$ are derived indicating a enough strength to promote necessary conditions to organize and maintain long-lived convective structures. Figure 12c shows the 12 UTC Palma sounding that is representative of the “tropical sounding” (McCaul, 1987). A deep moist layer, up to 9 km above ground level, without a stable layer can be observed. The lapse rate is less than dry adiabatic but greater than moist adiabatic, i.e., the sounding could indicate conditional instability. Without a capping inversion, but with a deep moist layer, there is the possibility of widespread convection. In fact, the daily precipitation became organized recording rainfall up to 200 mm over Balearic zone and up to 90 mm over Melilla.

The convective available potential energy (CAPE) and the convective inhibition (CIN) are also important parameters to capture moisture and conditional instability information (Zawadzki et al., 1981). The CAPE reflects the intensity of vertical motions of individual air parcels and is therefore a variable that indicates the strength of convective systems. High values of CAPE are indicative of possible high precipitation rates. The CIN is the work needed to lift an air parcel from rest at the surface to the level of free convection. It is a measure of the strength of the cap when a stable layer or capping inversion is present. High derived CIN values are conducive to lower-level channelling of the moist air masses towards the western Mediterranean area. The CIN values at the two stations, decreasing from 400 J $kg^{-1}$ on 8 November to nearly zero on 10 November, together with values in CAPE higher than 1600 J $kg^{-1}$ resulted on strong lifting needed to initiate deep convection. Figure 13 displays a CAPE distribution at 0000 and 1200 UTC over the western Mediterranean area. It can be noted how the index value increase throughout the episode extending the affected zone from Algeria, on 9 November with values higher than 1000 J $kg^{-1}$, to the Balearic area on 11 November with values of up to 800 J $kg^{-1}$. The remainder dates (not shown) of the episode were borne CAPE values of 200-400 J $kg^{-1}$ over the Spanish Mediterranean coast favouring the further development of precipitating systems over such area.

## 6. Summary and discussion

A mesoscale numerical analysis of a severe flash flood event in the western Mediterranean area is studied. The first step in this paper has been the objective selection of such event by means of the SVDA applied to the western Mediterranean precipitation and the large-scale atmospheric variables. To characterise the atmospheric circulation, 300-hPa geopotential height and meridional wind components of 54 autumns (September-October-November) from 1948 to 2001 have been used. For the same period, 26 precipitation time series covering eastern Iberia and the Balearic Islands have been considered. From the diagonalisation of the three matrices (Z300-PCP), (U300-PCP) and (V300-PCP), two leading modes were obtained suggesting that the large-scale atmospheric circulation at 300 hPa is responsible of much of the signal related to the western Mediterranean precipitation.

The heavy rain episode has been extracted from the second mode of covariability for the three diagonalisations and it explains more than 21% of the squared covariance between large-scale and precipitation fields. Both large-scale and precipitation expansion coefficient series exceed more than two standard deviations at November 2001 indicating high degree of coupling between the large-scale variables and regional precipitation. From this date, the heavy rainfall case was analysed by identifying and evaluating both large-scale setting and mesoscale processes involved in the case study by means of the non-hydrostatic mesoscale model, MM5, presented in the methodology section. The corresponding daily data for November 2001 indicated that besides the episode covered from 8 to 21 November 2001, the heavy precipitation basically occurred from 8 to 12 November and mainly affected the northern of Africa, Balearic Islands and E-SE Spanish coast, with particularly heavy 24-h rainfall totals on 10 and 11 November at Algeria.

The second SVD mode showed that above-normal precipitation values over SE Iberia and the Balearic area are determined by the presence of a centre of positive geopotential anomalies in the eastern North Atlantic sandwiched by two negative anomaly centres. The corresponding SVD patterns of both zonal and meridional wind components are dynamically coherent with the geopotential configuration indicating that the mode of the three SVD analyses represents a well-defined large-scale atmospheric structure. On the other hand, the main synoptic-scale features of the flash flood event showed a persistent and particular configuration corresponding to the presence of a long-lived Ω blocking geopotential pattern with a zonally oriented configuration of a high sandwiched in between two lows at surface and with a stationary ridge laying eastern Atlantic Ocean and a main trough situated over the western Mediterranean zone at upper level. It was remarkable the similarity between the obtained statistically mode with monthly data and the daily real synoptic configuration highlighting the strength of the link synoptic variables-regional precipitation and revealing that the methodology was been able to capture such catastrophic flash flood event.

The large-scale setting also showed at 300 hPa the presence of a jet streak promoting additional unstable conditions over the western Mediterranean area. If a

jet stream advects colder air along its axis, stratospheric air descends along the upper frontal zone into the midtroposphere. Under such conditions, some of that air then moves along cyclonically curved horizontal trajectories that eventually ascend east of the cyclone (Muller and Fuelberg, 1990). The air mass marked by high PV, as in the November 2001, can be stretched to increase relative vorticity, which augments deepening of a cyclone, especially when a low-level diabatic source of PV is present in the same area. For the November 2001 event, the modulation of the air masses and the Atlas Mountains ridge was also intensified with the intense upper level winds. In this event, ahead of the PV anomaly, the increase of positive vorticity advection with height favoured vertical upward motions.

Throughout the event, the evolution of several convective storm indices for Murcia and Palma stations were also derived showing values corresponding to high potential for convective storms. Soundings for these stations were also analysed indicating increase in conditional instability due to deep moist layers as well as moderate to strong vertical wind shear of horizontal wind persisting during the heavy rainfall period. Moreover, CAPE and CIN values obtained for the episode were diagnosed showing values indicative of severe storms. CAPE (CIN) values of 800 $Jkg^{-1}$ (nearly zero) were derived over the Balearic area and CAPE values higher than 1000 J $kg^{-1}$ were obtained over northern Africa resulting on very strong lifting needed to initiate and develop deep and intense convection.

The explosive storm development over the western Mediterranean area was due to a number of factors all coming together at the same place and time. The contribution from the large-scale conditions was crucial. A synoptic critical control was the blocking omega pattern that promoted the channelling effect. This synoptic scenario acted to induce mass ascent and release of conditional instability. Moreover, the lifting on the Atlas Mountain and the Balearic orography together with the front associated with the main low contributed to additional airmass ascent and subsequently severe weather.

*Acknowledgements*
*This work has been supported by the research projects REN2003-03647 and CGL2004-01584/CLI. The authors wish to thank the Spanish Meteorological Service (INM: Instituto Nacional de Meteorología) for providing the precipitation dataset and the NOAA-CIRES Climate Diagnostics*

*Center, Boulder, Colorado, USA from their Web site at http://www.cdc.noaa.gov for providing the NCEP Reanalysis data.*

# REFERENCES

Anthes RA. and Warner TT. 1978. Development of hydrodynamic models suitable for air pollution and other mesometeorological studies. *Mon. Wea. Rev.,* **106**, 1054-1078.

Barnes SL. and Colman BR. 1994. Diagnosing an operational numerical model using *Q*-vector and potential vorticity concepts. *Wea. Forecast.*, **9**, 85-102.

Benjamin SG. 1983. *Some effects of heating and topography on the regional severe storm environment*. Ph.D. Thesis. The Pennsylvania State Univ. 265 pp.

Betts AK. 1986. A new convective adjustment scheme. Part I: Observational and theoretical basis. *Quart. J. Roy. Meteor. Soc.*, **112**, 677-692.

Betts AK. and Miller MJ. 1986. A new convective adjustment scheme. Part II: Single column tests using GATE wave, BOMEX,ATEX and Artic air-mass data sets. *Quart. J. Roy. Meteor. Soc.*, **112**, 693-709.

Blackadar AK. 1979. High resolution models of the planetary boundary layer. *Advances in Environmental Science and Engineering*, **1**, Nº 1, Pfafflin J. and Ziegler E. (Eds)., Gordon and Breach, 50-85.

Bluestein H B. 1993. *Synoptic Dynamic Meteorology in Midlatitudes.Vol. II. Observations and Theory of Weather Systems*. Oxford University Press. 594pp.

Bretherton C S, Smith C, Wallace J M. 1992. An intercomparison of methods for finding coupled patterns in climate data. *J. Clim.*, **5**, 541-560.

Corte-Real J, Zhang X, Wang X. 1995. Large-scale circulation regimes and surface climatic anomalies over the Mediterranean. *Int. J. Climatol.*, **15**, 1135-1150.

Davis R. 1976. Predictability of sea surface temperature and sea level pressure anomalies over the Northern Hemisphere. *J. Phys. Ocean.*, **6**, 249-266.

Doswell III CA, Ramis C, Romero R, Alonso S, 1998. A diagnostic study fo three heavy precipitation episodes in the Western Mediterranean Region. *Wea. Forecast.*, **13**, 102-124.

Font I .2000. *Climatología de España y Portugal*. 2nd edn. Ediciones Universidad de Salamanca, Spain. 422pp.

Galway JG. 1956. The lifted index as a predictor of latent instability. *Bull. Am. Meteorol. Soc.*, **37**, 528-529.

George JJ. 1960. *Weather forecasting for aeronautics*, Academic Press.

Grell GA, Dudhia and Stauffer DR. 1994. Diagnosing coupled jet streak circulations for a northern plains snow band from the operational nested-grid model. *Wea. Forecast.*, **7**, 26.48.

Heyen H, Zorita E, von Storch.1996. Statistical downscaling of monthly mean North Atlantic air-pressure to sea level anomalies in the Baltic Sea. *Tellus*, **48A**, 312-323.

Holton J R. 1992. *An introduction to dynamic meteorology*. 3rd Ed. Int. Geophys. Ser, 48. Adademic Press, 511pp.

IPCC Technical Summary. Climate Change. 2001. *Impacts, Adaptation and Vulnerability. A Report of Working Group II of the Intergovernmental Panel on Climate Change*. J J. McCarthy, O F. Canziani, N A. Leary, D J. Dokken and K S. White (Eds). Cambridge University Press, 1000pp.

Kain JS. and Fritsch JM. 1990. A one-dimensional entraining/detraining plume model and its application in convective parameterization. *J. Atmos. Sci.*, **47**, 2784-2802.

Kalnay E, Kanamitsu M, Kistler R, Collins D, Deaven D, Gandin L, Iredell M, Saha S, White G, Woolen J, Zhu Y, Chelliah M, Ebisuzaki W, Higgins W, Janowiak J, Mo K C, Kopelewski C, Wang J, Leetmaa A, Reynolds R, Jeene R and Jsoseph D. 1996. The NCEP/NCAR 40-years Reanalysis, Project. *Bull. Amer. Meteorol. Soc.*, **77**, No. 3: 437-471.

Klemp J.B. and R.B. Wilhelmson 1978. Simulations of right-and left-moving storms produced through storm splitting. *J. Atmos. Sci.*, **35**, 1097-1110.

Linés A. 1970. The climate of the Iberian Peninsula. *World survey of climatology*, **5**, *Climate of Northern and western Europe*. CC Wallen, (Ed). Elsevier, Dordrecht, 195-239.

Lorenz E. 1956. *Empirical orthogonal functions and statistical weather prediction*. Sci. Rept. no. 1, Statistical forecasting Project, Dept. of Meteor., MIT, Cambridge, Mass, 49pp.

Maheras P. 1988. Changes in precipitation conditions in the Western Mediterranean over the last century. *J. Climatol.*, **8**, 179-189.

McCaul EWJr. 1987. Observations for th hurricane “Danny” tornado outbreak of 16 August 1985. *Mon. Wea. Rev.*, **115**, 1206-1223.

McGinley, J. 1986. *Nowcasting mesoscale phenomena*. Mesoscale Meteorology and Forecasting, 657-688pp.

Martín ML, Luna MY , Morata A. and Valero F. 2004. North Atlantic teleconnection patterns of low-frequency variability and their links with springtime precipitation in the western Mediterranean. *Int. J. Climatol.,* **24**, 213-230.

Miller RC. 1972. *Notes on analysis and severe-storm forecasting procedures for the Air Force Global Weather Central.* Air Weather Service Tech. Rep., **200**, Air Weather Service, Scott Air Force Base.

Muller BM and Fuelberg HE. 1990. A simulation and diagnostic study of water vapor image dry bands. *Mon. Wea. Rev.*, **118**, 705-722.

Reisner, J., Rasmussen R. M., and Bruintjes R. T. 1998. Explicit forecasting of supercooled liquid water in winter storms using the MM5 mesoscale model. *Quart. J. Roy. Meteor. Soc.*, **124**, 1071-1107.

Romero R, Ramis C. and Alonso, S. 1997. Numerical simulation of an extreme rainfall event in Catalonia: Role of orography and evaporation from the sea. *Quart. J. Roy.Meteor. Soc.*, **123**, 537-559.

Romero R, Ramis C, Alonso S. Doswell III CA and Stensrud DJ. 1998. Mesoscale model simulations of three heavy precipitation events in the western Mediterranean region. *Mon. Wea. Rev.*, **126**, 1859-1881.

Romero R, Doswell III CA, Ramis C. 2000. Mesoscale numerical study of two cases of long-lived quasistationary convective systems over Eastern Spain. *Mon. Wea. Rev.*, **128**, 3731-3751.

Smith RB. 1989. Hydrostatic airflow over mountains. *Advances in Geophysics*, **31**, Academic Press, 1-41.

Storch H von, Zwiers F W. 1999. *Statistical analysis in climate research*. Cambridge Univesity Press, UK.

Sumner E J 1954. A study of blocking in the Atlantic-European sector of the northern hemisphere. *Q. J. R. Meteorol. Soc.* , **80**, 402-416.

Sumner G, Homar V, Ramis C. 2001. Precipitation seasonality in eastern and southern coastal Spain. *Int. J. Climatol.,* **21**, 219-247.

Valero F, Luna M Y, Martín M L. 1997. An overview of a heavy rain event in southeastern Iberia: the role of large-scale meteorological conditions. *Ann. Geophys.*, **15**, 494-502.

Valero F, Luna MY, Martín ML, Morata A, González-Rouco F. 2004. Coupled modes of large-scale climatic variables and regional precipitation in the Western Mediterranean in autumn. *Clim. Dyn.*, **22**, 307-323.

Wheeler DA.1989. Meteorological gatherings from Spain. *Wheather*, **44(1)**, 12-20.

Zawadzki I, Torlaschi E. and Sauvageau R. 1981. The relationship between mesoscale thermodynamic variables and convective precipitation. *J. Atmos. Sci.*, **38**, 1535-1540.

Zhang DL and Anthes RA. 1982. A high-resolution model of the planetary boundary layer. Sensitivity tests and comparisons with SESAME-79 data. *J. Appl. Meteor*., **21**, 1594-1609.

Zhang DL and Fritsch JM. 1986. Numerical simulation of the meso-β scale structure and evolution of the 1977 Johnstown flood. Part I: Model description and verification. *J. Atmos. Sci*., **43**, 1913-1943.

Zhang DL, Chang HR, Seaman NL, Warner TT. and Fritsch JM. 1986. A two-way interactive nesting procedure with variable terrain resolution. *Mon. Wea. Rev.*, **114**, 1330-1339.

# Figure captions

Figure 1: Western Mediterranean basin indicating locations of precipitation stations by dots. The line AB indicates the direction of the vertical cross section discussed in the text.

Figure 2: The expansion coefficient time series of the second SVD mode between (a) Z300 and (b) precipitation; (c) U-wind and (d) precipitation; (e) V-wind and (f) precipitation. Units are in standard deviations.

Figure 3: Heterogeneous anomaly patterns of the second SVD mode: (a) Z300 pattern (contour interval is 10 gpm), and (b) its precipitation pattern; (c) U-wind pattern (contour interval is 1 $ms^{-1}$) and (d) its precipitation pattern and (e) V-wind pattern (contour interval is 1 $ms^{-1}$) and (f) its precipitation pattern. The contour interval for the precipitation patterns is 5 mm. The positive (negative) contours are solid (dashed).

Figure 4: The used centred fine grid domain and its orography.

Figure 5: The selected coarse domain centred at the same location of Figure 2.

Figure 6: Accumulated precipitation from 8 November to 13 November 2001 at 1200 UTC in the western Mediterranean basin. Contours every 50 mm, starting in 50 mm.

Figure 7: Synoptic situation at 1200 UTC on 9 November 2001. (a) Surface analysis (pressure contours every 4 hPa); (b) 500 hPa analysis (height contours, every 60 m, are shown by continuous lines; temperature contours, every 4ºC, are indicated by dashed lines) and (c) 300 hPa analysis (height contours, every 120 m, are shown by continuous lines; vector wind field with the reference vector in the lower right corner representing 80 $ms^{-1}$).

Figure 8: Distribution of air temperature at 2 m on 10 November 2001 at 1200 UTC in the fine grid domain of the model. Contours every 4ºC.

Figure 9: Diagnosed Potential Vorticity at 300 hPa, 1200UTC: (a) 8 November; (b) 9 November; (c) 10 November; (d) 11 November and (e) 12 November 2001. Interval contour is 2 PVU ($10^{-6}$ $m^2$ $s^{-1}$ K $kg^{-1}$) starting in 2 PVU.

Figure 10: Vertical cross section along AB (see Figure 1) showing relative humidity (contours every 20%, starting in 40, dashed line) and upward vertical velocity (contour interval is 0.4 $ms^{-1}$, starting in 0.4, continuous line).

Figure 11: Relative humidity (in %) on 11 November 2001, 1200 UTC, at 500 hPa.

Figure 12: Skew-T diagram representing the observations measured by the radiosonde launched in Palma de Mallorca (a) on 9 November at 0000 UTC,(b) on 10 November at 0000UTC and (c) 11 November at 1200 UTC. Solid line is the temperature plot (ºC), dashed line is the dewpoint plot (ºC); windbarbs reflect the observed wind direction and speed (half line = 5 knots; total line = 10 knots and flag = 50 knots).

Figure 13: Spatial distribution of CAPE (a) on 9 November 2001 at 1200 UTC and (b) 11 November 2001 at 0000 UTC. Isopleth interval is 500 $Jkg^{-1}$.

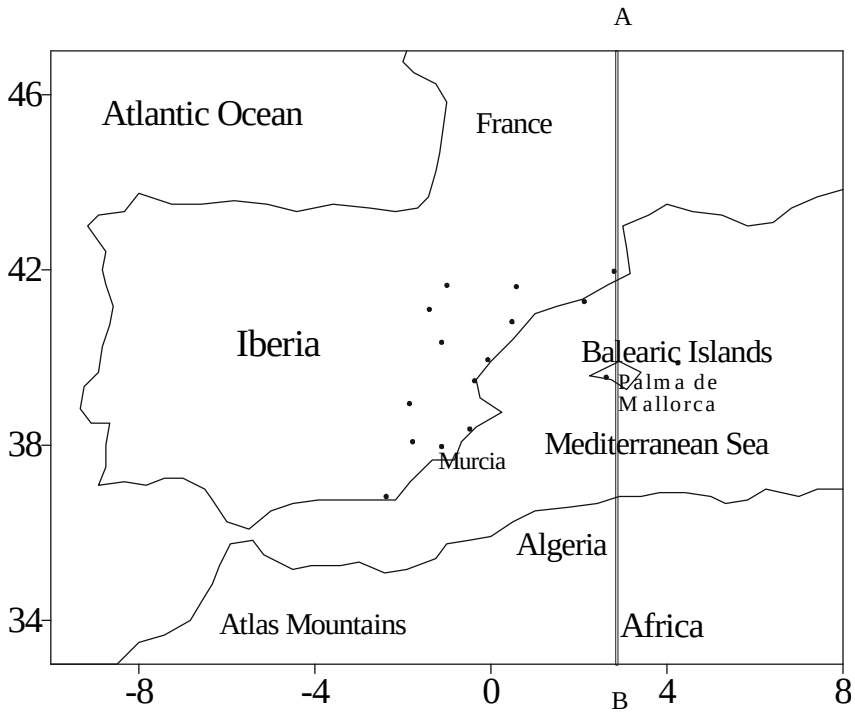
A
46
42
38
34
Atlantic Ocean
France
Iberia
Balearic Islands
Palma de
Mallorca
Mediterranean Sea
Murcia
Algeria
Atlas Mountains
Africa
-8
-4
0
B
4
8

Figure 1

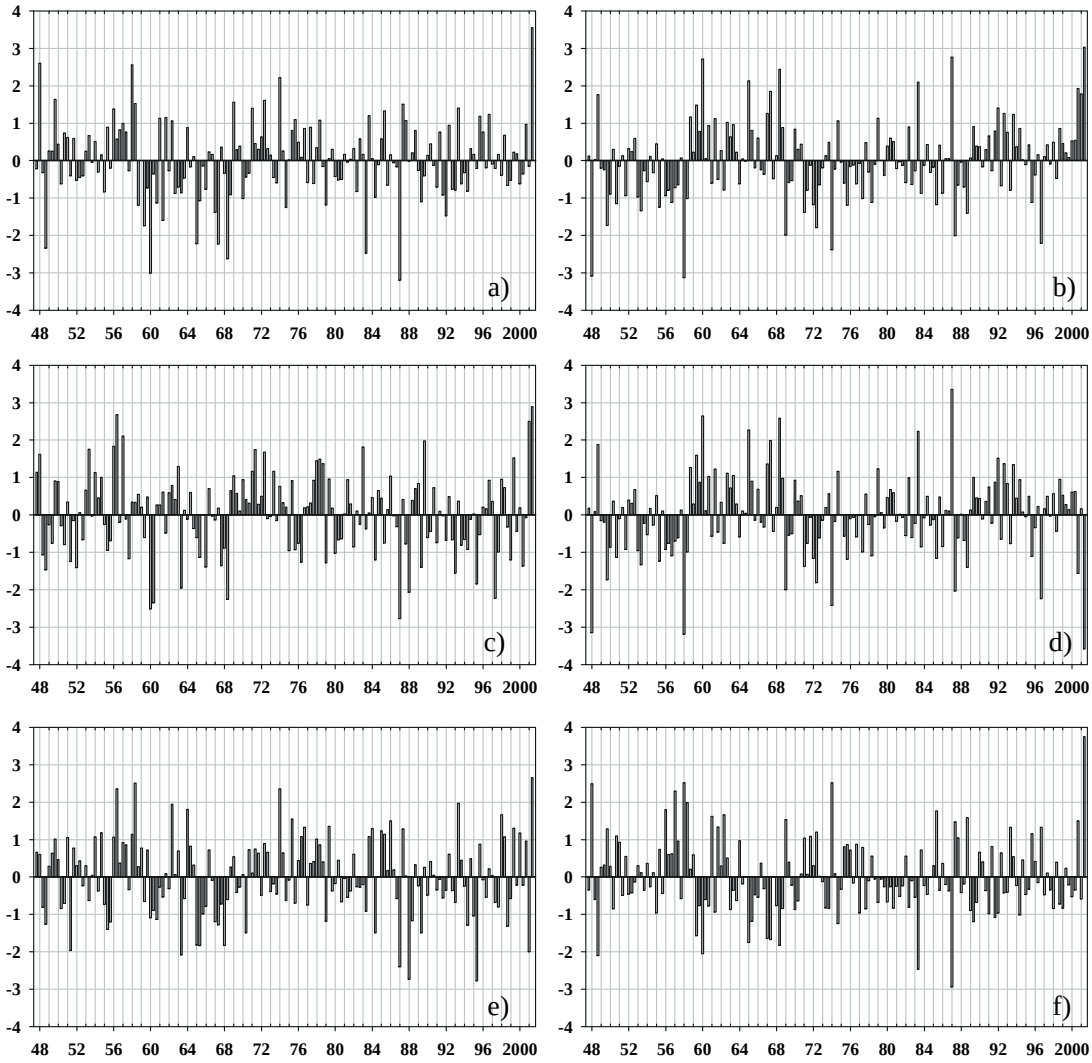


Figure 2

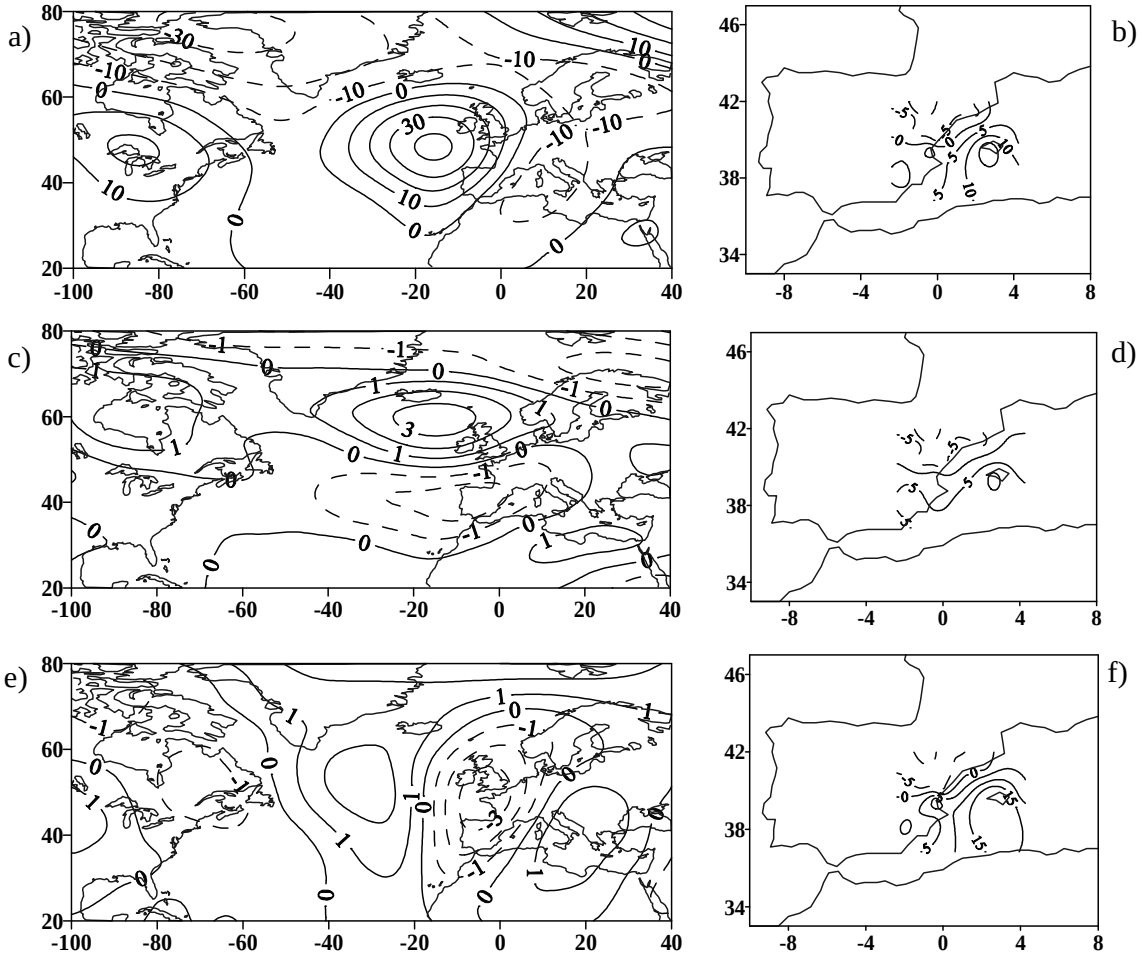


Figure 3

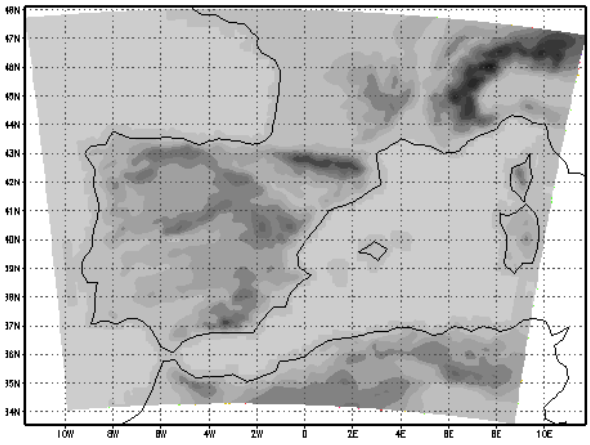
48N
47N
46N
45N
44N
43N
42N
41N
40N
39N
38N
37N
36N
35N
34N
10W
8W
6W
4W
2W
0
2E
4E
6E
8E
10E

Figure 4

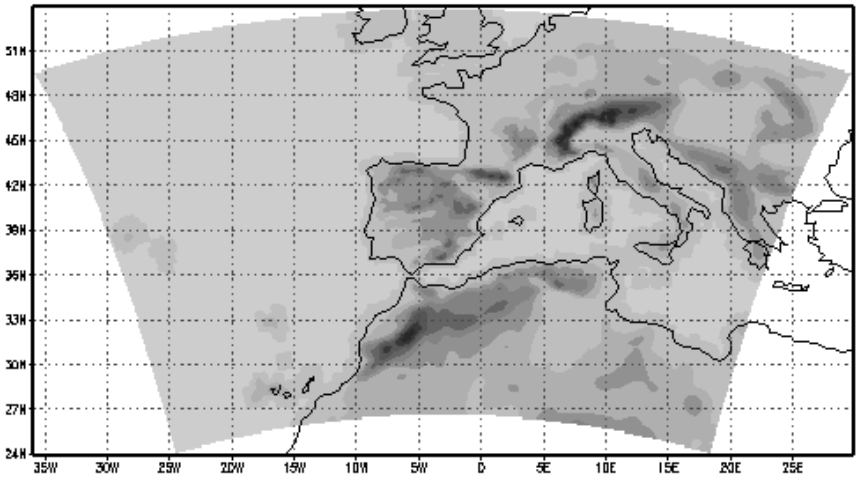
51N
48N
45N
42N
39N
36N
33N
30N
27N
24N
35W
30W
25W
20W
15W
10W
5W
0
5E
10E
15E
20E
25E

Figure 5

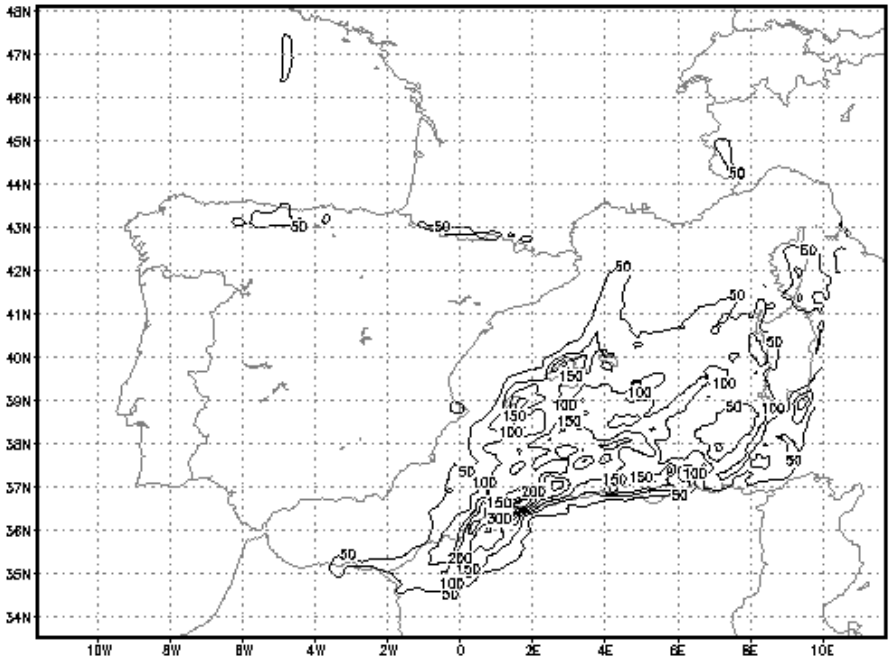
48N
47N
46N
45N
44N
43N
42N
41N
40N
39N
38N
37N
36N
35N
34N
10W
8W
6W
4W
2W
0
2E
4E
6E
8E
10E

Figure 6

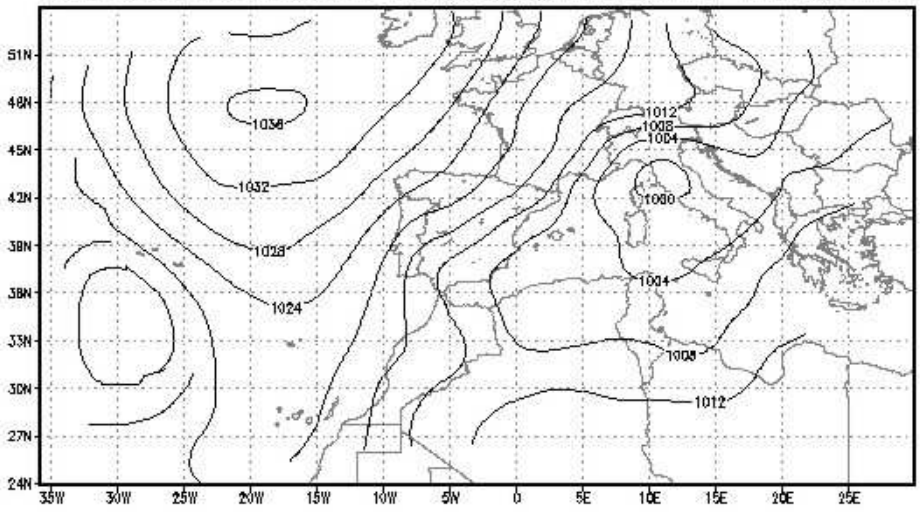
51N
48N
45N
42N
39N
36N
33N
30N
27N
24N
35W
30W
25W
20W
15W
10W
5W
0
5E
10E
15E
20E
25E
1036
1032
1028
1024
1012
1008
1004
1000
996
1008
1012

a)

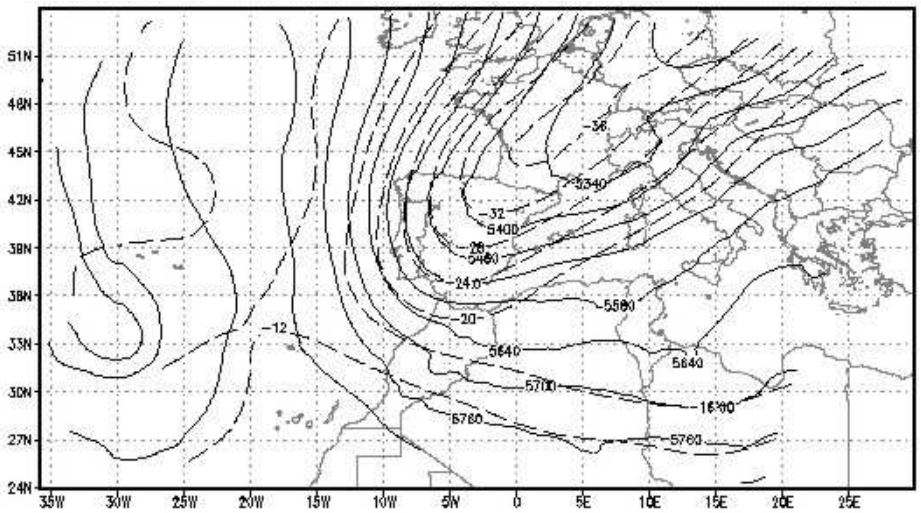
51N
48N
45N
42N
39N
36N
33N
30N
27N
24N
35W
30W
25W
20W
15W
10W
5W
0
5E
10E
15E
20E
25E
-56
-5340
-32
5400
-28
5460
-24
5520
5580
-20
-12
5640
5700
5760
5640
5760

b)

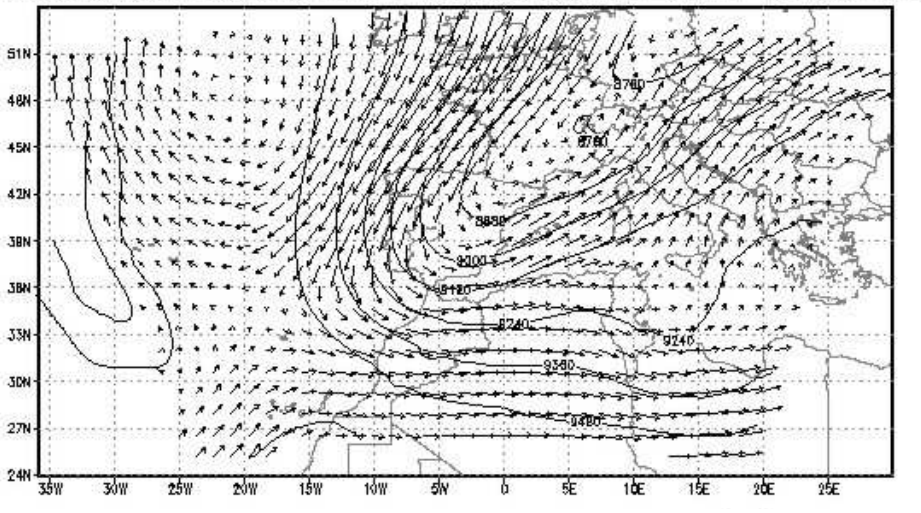
51N
48N
45N
42N
39N
36N
33N
30N
27N
24N
35W
30W
25W
20W
15W
10W
5W
0
5E
10E
15E
20E
25E
8760
8760
8880
9000
9120
9240
9360
9480
9240

c)

Figure 7

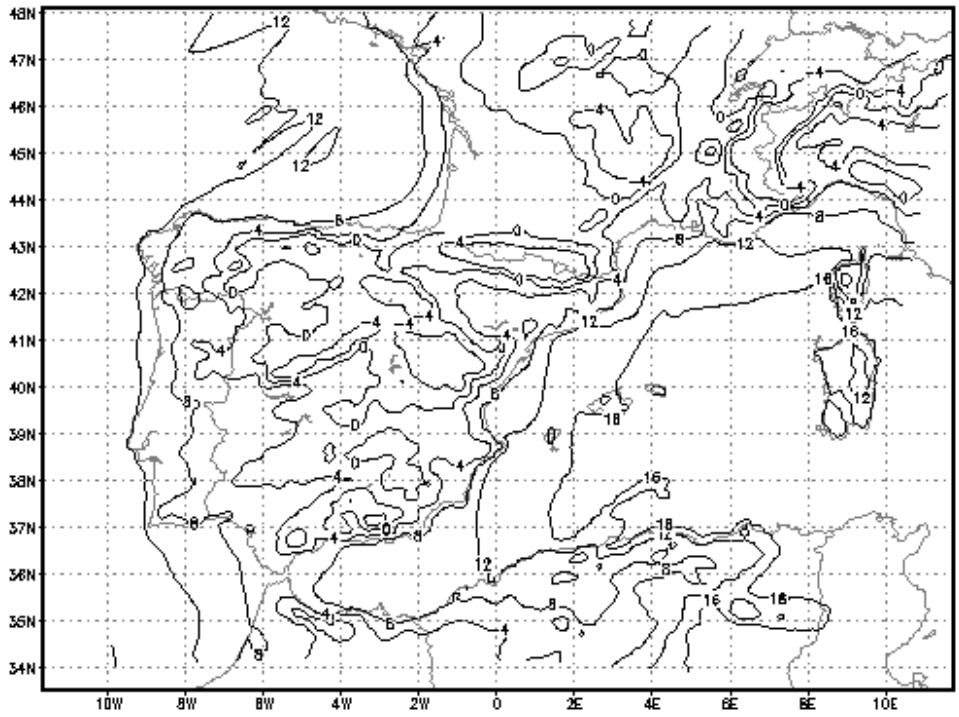
48N
47N
46N
45N
44N
43N
42N
41N
40N
39N
38N
37N
36N
35N
34N
10W
8W
6W
4W
2W
0
2E
4E
6E
8E
10E

Figure 8

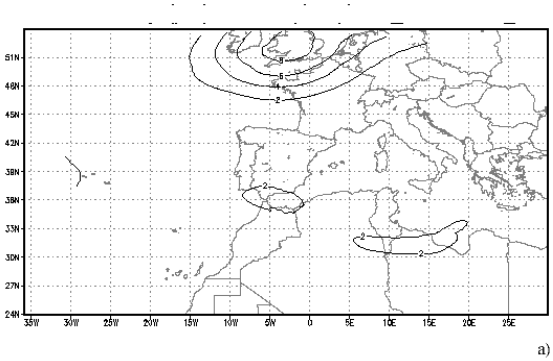


a)

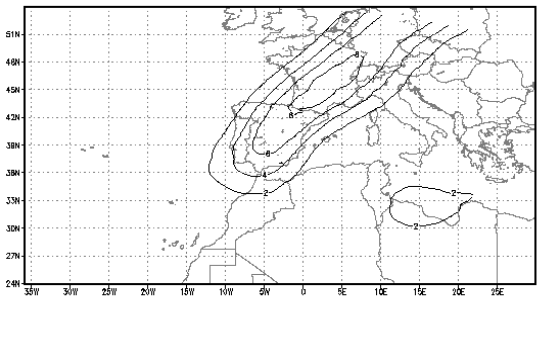


b)

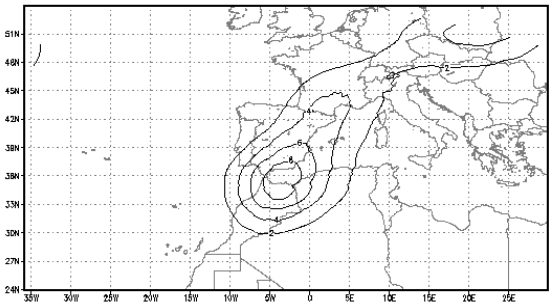


c)

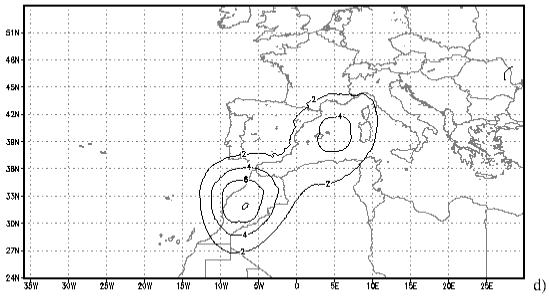


d)

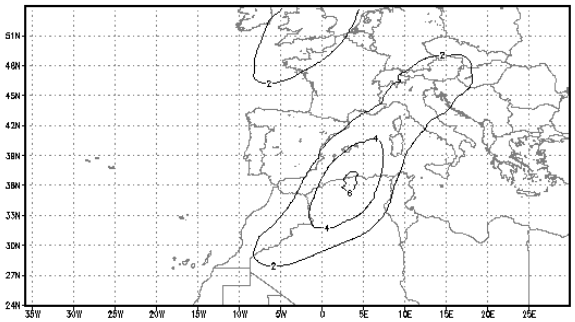


e)

Figure 9

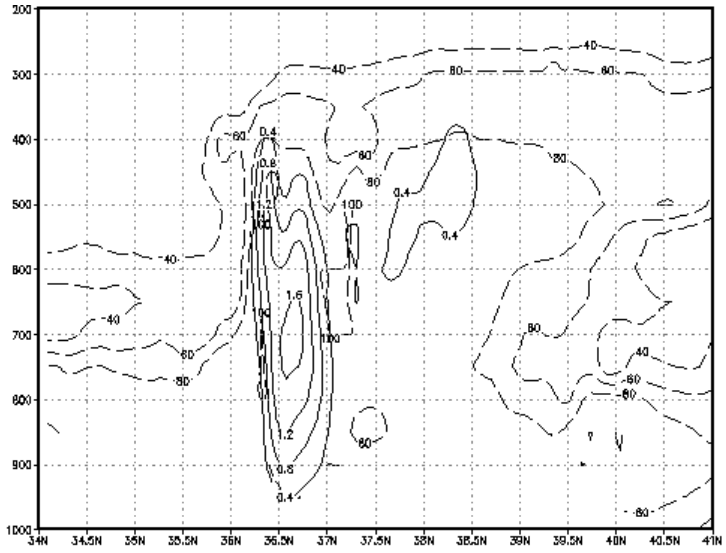
200
300
400
500
600
700
800
900
1000
34N
34.5N
35N
35.5N
36N
36.5N
37N
37.5N
38N
38.5N
39N
39.5N
40N
40.5N
41N

a)

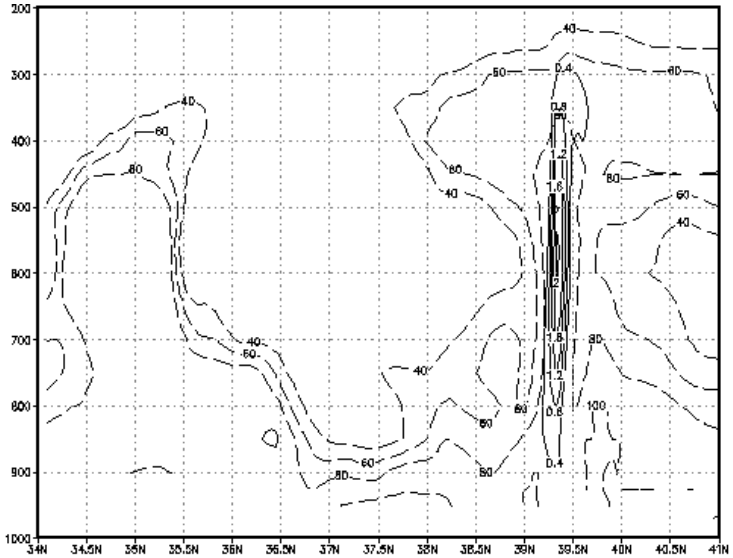
200
300
400
500
600
700
800
900
1000
34N
34.5N
35N
35.5N
36N
36.5N
37N
37.5N
38N
38.5N
39N
39.5N
40N
40.5N
41N

b)

Figure 10

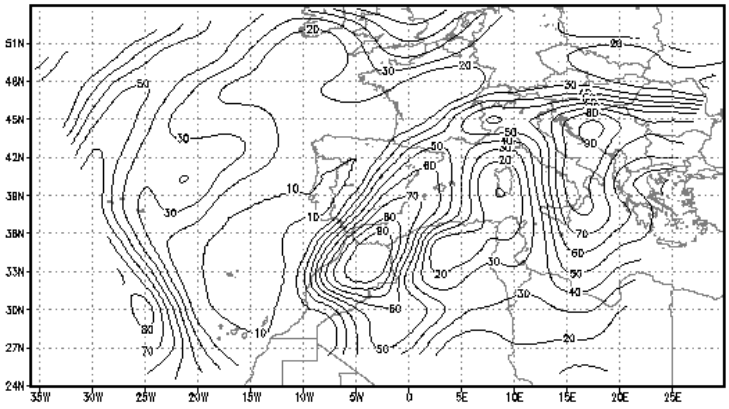
51N
48N
45N
42N
39N
36N
33N
30N
27N
24N
35W
30W
25W
20W
15W
10W
5W
0
5E
10E
15E
20E
25E

Figure 11

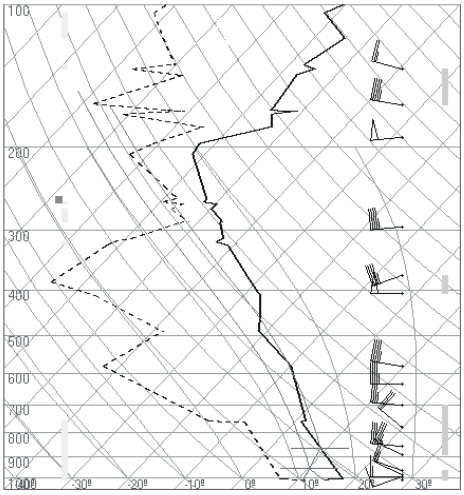


a)

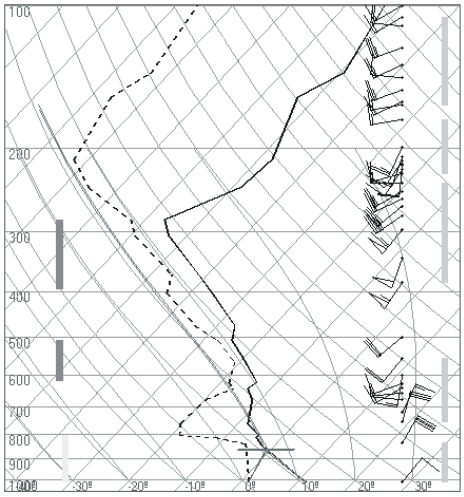


b)

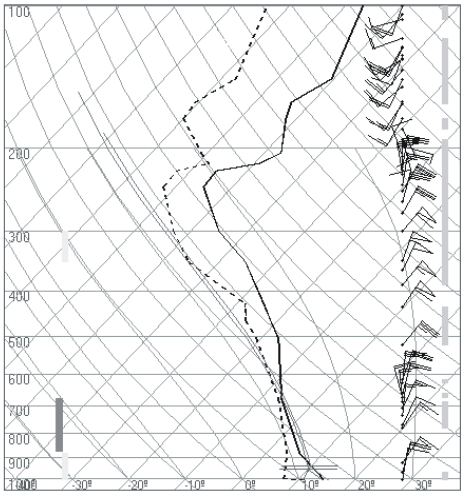


c)

Figure 12

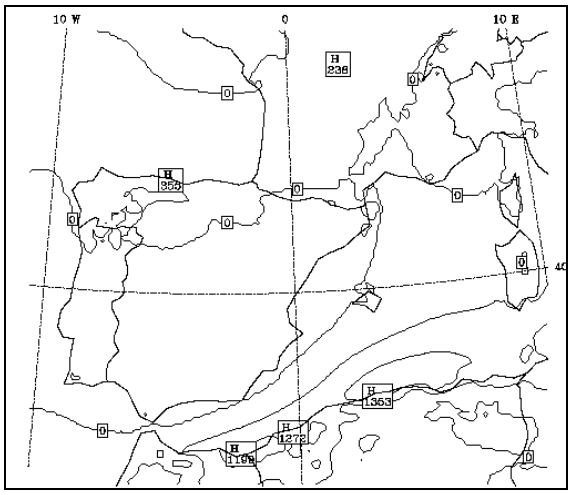
10 W
0
10 E
H
336
H
355
H
1353
H
1276
H
1198
0

a)

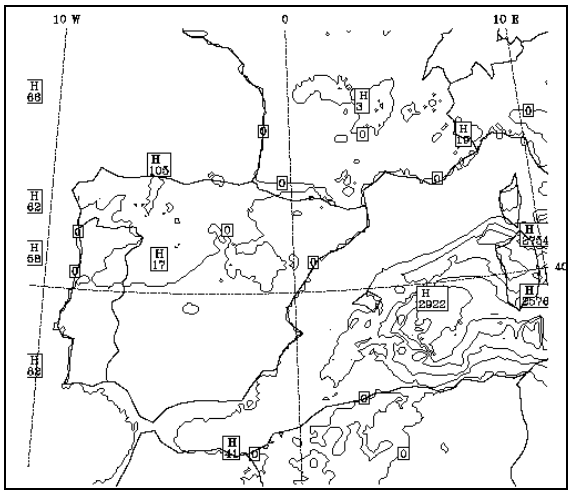
10 W
0
10 E
H
68
H
62
H
58
H
62
H
105
H
17
H
3
H
19
H
2922
H
41
0

b)

Figure 13